JOURNAL OF NATURAL PRODUCTS

Article

pubs.acs.org/jnp

Cytotoxic Dimeric Epipolythiodiketopiperazines from the Ascomycetous Fungus *Preussia typharum*

Lin Du,[†,‡,§,⊥] Andrew J. Robles,[∇,⊥] Jarrod B. King,[†,‡,§] Susan L. Mooberry,*[,‡,∇,∥,#] and Robert H. Cichewicz*[,†,‡,§]

[†]Natural Products Discovery Group, [‡]Institute for Natural Products Applications and Research Technologies, and [§]Department of Chemistry and Biochemistry, Stephenson Life Sciences Research Center, 101 Stephenson Parkway, University of Oklahoma, Norman, Oklahoma 73019-5251, United States

[∇]Department of Pharmacology, [∥]Cancer Therapy & Research Center, and [#]Department of Medicine, University of Texas Health Science Center at San Antonio, 7703 Floyd Curl Drive, San Antonio, Texas 78229, United States

Supporting Information

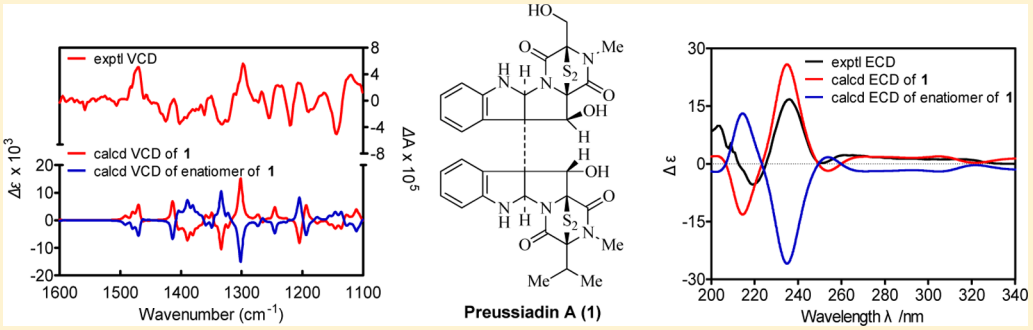

ABSTRACT: Two new dimeric epipolythiodiketopiperazines, preussiadins A (**1**) and B (**2**), together with two known diastereomers, leptosins C (**6**) and A (**7**), were obtained from the mycelia of a *Preussia typharum* isolate. The structures of the new compounds were established by spectroscopic methods, and the absolute configurations of **1** and **2** were assigned by chemical transformations and comparisons of quantum chemical ECD and VCD calculations to experimental data. Compound **1** exhibited potent cytotoxic activity in the NCI-60 cell line panel with an average LC_{50} value of 251 nM. Further studies demonstrated that **1** circumvents P-glycoprotein-mediated drug resistance, yet had no significant antitumor activity in a xenograft UACC-62 melanoma model.

The epipolythiodiketopiperazine (ETP) alkaloids represent a large family of fungal secondary metabolites with potent cytotoxic activities.[1,2] Recently, ETP alkaloids have been reported to inhibit a variety of cellular targets and signaling processes including topoisomerases I and II, Akt, and protein−protein interactions critical for cancer cell growth including the interaction between HIF1-α and p300.[3−15] Some of the ETPs were also found to inhibit the growth of tumor xenografts in mice.[4−7,10,12] One of the most widely studied ETPs, chaetocin, has displayed a wide spectrum of *in vivo* antitumor activities against SK-OV-3 human ovarian cancer,[4] U937 human leukemia,[5] RPMI 8226 human myeloma,[6] and mouse and human hepatomas.[10] These observations suggest the ETPs may have utility as lead molecules for drug development and/or molecular tools. In this report, we describe the isolation, structural determination, absolute configuration assignments, and conformational analyses of two new ETPs, preussiadins A (**1**) and B (**2**), together with two known diastereomers, leptosins C (**6**) and A (**7**), from *Preussia typharum*. We also investigated the *in vitro* cytotoxicity of these compounds, as well as the *in vivo* antitumor efficacy of **1**.

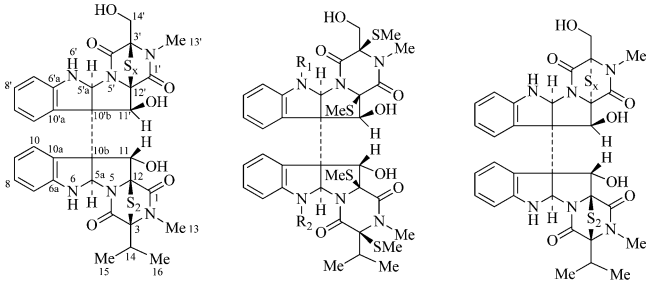

RESULTS AND DISCUSSION

Preussiadin A (**1**) was obtained as a white, amorphous powder from a *P. typharum* isolate that originated from a bottomland-forest-derived soil sample.[16] Its molecular formula was established

Received: March 10, 2014
Published: June 3, 2014

dx.doi.org/10.1021/np5002253 | *J. Nat. Prod.* 2014, 77, 1459−1466

as $C_{32}H_{32}N_6O_7S_4$ by HRESIMS, indicating 20 degrees of unsaturation. The IR spectrum confirmed the presence of amide (ν_{max} 1673) and hydroxyl (ν_{max} 3399) groups. The ^{1}H NMR spectrum displayed characteristic resonances attributable to two ABCD aromatic systems (δ_H 5.71−7.70, 8H) (Table 1). Analysis of the ^{13}C NMR and ^{1}H−^{13}C HSQC spectra enabled the assignment of the 32 carbon resonances to four methyl groups including two *N*-methyls (δ_C 27.5 and 28.0), 13 methines, one oxygenated methylene (δ_C 60.7), four carbonyls (δ_C 167.6, 160.7, 165.5, and 163.1), and 10 additional quaternary carbons (Table 1). Further analysis of the 1D (^{1}H and ^{13}C) and 2D (HMBC) NMR data (Table S1) enabled the determination that **1** was a new dimeric ETP, which was a diastereomer of leptosin C (**6**).[17] The ^{13}C NMR data for **1** and **6** were nearly superimposable for the lower monomeric unit (C-1−C-16); however, significant variation occurred (>2 ppm changes) among the chemical shifts assigned to the C-1′, C-3′, C-4′, C-5a′, and C-11′ resonances for the upper monomeric portion. We surmised that this was due to a change in the absolute configuration of the diketopiperazine system in the upper half of the molecule. To investigate this in greater detail, **1** was subjected to cleavage of the disulfide bond followed by *S*-methylation.[17] In addition to the expected product **3**, two minor *N*-methylated products, **4** and **5**, were also obtained. The planar structure of **3** was confirmed by analysis of its HRESIMS and 1D (^{1}H and ^{13}C NMR, Tables 1 and 2) and 2D (HSQC and HMBC, Table S3) NMR data. The *N*-methylation patterns of **4** and **5** were determined by comparisons of the ^{1}H and ^{13}C (Table 1) NMR data with those of **3**. Significant downfield shifts were observed for C-5a′ or C-6a′ and C-5a or C-6a due to the *N*-methylation of their respective adjacent nitrogen atoms in **4** and **5**, respectively. The relative configuration of **3** was established as shown in Figure 1 based on ROESY correlation data (H-11 to *S*-Me-12, H-10, H-11′; H-10 to H-10′, OH-11′; OH-11′ to H-10′, *S*-Me-12′; OH-11 to H-11′, H-5a′; H-5a′ to H-5a, Me-16). Thus, the configuration assignments for **3** enabled us to infer the inversion of C-3′ and C-12′ in **1** relative to the remaining portions of the molecule. This confirmed that metabolite **1** was a diastereomer of leptosin C (**6**).

The independent assignment of the absolute configuration of **1** was initially hindered when all attempts to crystallize the compound and its derivatives proved unsuccessful. Alternatively, quantum chemical computational calculations were carried out to generate theoretical VCD and ECD spectra, as well as a specific rotation value for **1**. A conformational search was carried out with Spartan'10 at the molecular mechanics level (MMFF)[18] based on the proposed absolute configuration 3*S**, 5a*R**, 10b*S**, 11*S**, 12*S**, 3′*R**, 5′a*S**, 10′b*R**, 11′*S**, 12′*R**. Geometry, frequency, specific rotation, and IR and VCD intensity calculations of the 20 lowest energy conformers (within 5 kcal/mol) resulted from a conformational search carried out at the DFT level (B3LYP functional/6-31+G** basis set) with Gaussian 09.[19] The calculated frequencies were scaled by 0.975, and the IR and VCD intensities were converted to Lorentzian bands with a 6 cm^{-1} half-width for comparisons to experimental values.

Gaussian calculations resulted in six low-energy conformers within 2.7 kcal/mol of the lowest energy conformer, whereas all other conformers were more than 4.4 kcal/mol higher in energy. The IR and VCD spectra and specific rotations of the six conformers were summed based on a Boltzmann statistical weighting (Figure 2A). TD-DFT calculations (B3LYP functional/6-31+G** basis set) provided individual UV and CD spectra for the six conformers, which were then combined using SpecDis 1.60 (using a sigma value of 0.2 eV).[20] After applying a UV-shift correction of −50 nm, the theoretical CD spectra were compared with the experimental data (Figure 2B). In both cases, the calculated VCD (Figure 2A) and ECD (Figure 2B) spectra matched well with the experimental data. In addition, a positive specific rotation value was calculated for **1** ($[\alpha]_D$ 53), which was in agreement with the experimental observations ($[\alpha]^{24}_D$ 66). Therefore, the absolute configuration of **1** was determined to be 3*S*, 5a*R*, 10b*S*, 11*S*, 12*S*, 3′*R*, 5′a*S*, 10′b*R*, 11′*S*, 12′*R*.

Preussiadin B (**2**) was assigned a molecular formula of $C_{32}H_{32}N_6O_7S_6$ by HRESIMS, indicating the presence of two additional sulfur atoms in the molecule compared to **1**. The ^{1}H and ^{13}C NMR data (Tables 1 and 2) as well as HMBC correlations (Table S2) enabled us to confirm that **1** and **2** shared a majority of the same structural features. Further scrutiny of the NMR data revealed that the lower portions of molecules **1** and **2** were identical; however, the upper parts of the compounds exhibited some small, but perceptible changes that led us to conclude the two additional sulfur atoms formed a tetra-sulfide bridge between C-3′ and C-12′. The proposed structure and absolute configuration assignment for **2** was determined by subjecting the metabolite to the previously described *S*-methylation reaction. This provided three products (**3**−**5**) that were confirmed as being identical to the products of the cleavage/methylation reaction of **1**. Thus, we were able to confirm that both compounds **1** and **2** shared the same absolute configuration.

Two previously described dimeric ETPs, leptosins A (**7**) and C (**6**),[21] were also purified from the fungal extract. Fortuitously, the ^{1}H NMR spectrum of **6** exhibited some unusual features that ultimately led to further insights concerning the axial chirality of these compounds. In $CDCl_3$ at 25 °C, we observed broad proton resonances for **6** (Figure 3A) that we interpreted as arising from the interconversion of conformers. Using variable-temperature (VT) NMR experiments at −20, −40, and −60 °C, we succeeded in generating two distinct sets of sharpened proton signals (Figure 3). However, upon switching to acetone-d_6 as the solvent, we were able to generate a single major stereoisomer that was stabilized at low temperature (Figure 3B). This contrasted with data for **1**−**5** and **7**, in which only a single major stereoisomer was observed in $CDCl_3$. These results prompted us to further probe the axial chirality features of this class of compounds. ROESY experiments enabled us to directly deduce that **1** favored a *P* configuration, whereas **2** and **3** favored an *M* configuration under these experimental conditions (Tables S1 and S2 and Figures 1 and 4A). Whereas the assignments for **4**−**7** could not be directly extrapolated from the ROESY data, our results did generate an additional useful pattern that was evident in the ^{1}H NMR data. Namely, the ^{1}H NMR spectrum of **1** showed that H-10 was shifted upfield to δ_H 5.71 relative to H-10′ (δ_H 7.70) due to the shielding effect of phenyl ring B (Figures 4A and 4B). In contrast, H-10′ was observed in upfield positions for **2** (δ_H 5.85) and **3** (δ_H 5.78) due to shielding of phenyl group A (Figures 4A and 4B). Applying these observations to the remaining compounds in this series, we deduced that **4**−**6** adopted an *M* configuration, whereas **7** favored a *P* configuration (Figure 4).

The cytotoxic activities of **1**−**7** were initially tested in a human pancreatic cancer cell line (MIA PaCa-2). Compounds **1** and **2** were found to be the most potent, with IC_{50} values of 6.6 and 9.1 nM, respectively. Diastereomers **6** and **7** were determined to be nearly five times less potent, with IC_{50} values of 33.6 and 43.1 nM, respectively. Compounds **3**−**5** exhibited

Table 1. ^{1}H NMR Data of 1−5 (400 MHz, TMS, δ ppm)

	1[a]		2[a]		3[a]		4[a]		5[a]	
no.	δ_C	δ_H	δ_C	δ_H	δ_C	δ_H	δ_C	δ_H	δ_C	δ_H
1	167.6		167.4		165.8		165.9		165.9	
3	80.4		80.7		79.2		79.1		79.3	
4	160.7		160.6		164.7		164.7		164.6	
5a	79.0	5.96, s	80.4	5.77, s	79.7	5.76, d (3.0)	79.9	5.61, d (3.1)	86.1	5.62, s
6		5.46, s		4.64, s		4.45, d (2.9)		4.44, d (3.1)		
6a	148.2		150.0		151.1		151.2		153.5	
7	110.4	6.62, d (7.6)	110.0	6.42, d (7.6)	109.1	6.35, d (8.3)	109.1	6.35, d (7.4)	107.0	6.19, d (7.8)
8	130.4	7.08, t (7.0)	130.5	7.18, t (7.6)	129.9	7.14, td (7.7, 1.2)	129.9	7.15, td (7.7, 1.2)	130.0	7.20, td (7.8, 1.2)
9	119.9	6.45, t (7.7)	119.2	6.88, t (7.5)	118.4	6.82, td (7.5, 0.9)	118.4	6.80, td (7.5, 0.9)	117.3	6.76, td (7.4, 0.8)
10	125.3	5.71, d (7.7)	126.3	7.55, d (7.3)	125.6	7.72, d (7.5)	125.6	7.67, d (7.5)	125.2	7.65, d (7.4)
10a	126.3		127.1		128.4		128.5		128.7	
10b	65.4		64.6		63.1		63.0		62.2	
11	81.9	5.01, s	82.7	5.25, s	81.1	5.17, d (2.8)	81.1	5.14, d (3.0)	80.8	5.15, d (3.2)
12	75.2		75.5		72.5		72.6		72.9	
13	28.0	3.08, s	27.8	3.04, s	30.0	3.04, s	30.0	3.04, s	30.1	3.04, s
14	32.4	2.69, heptet (6.8)	32.4	2.68, heptet (6.8)	37.6	2.45, heptet (7.0)	37.5	2.45, heptet (7.0)	37.4	2.46, heptet (7.0)
15	18.1	1.44, br s	18.2	1.43, d (6.8)	18.2	1.23, d (7.0)	18.2	1.27, d (7.0)	18.2	1.24, d (6.8)
16	18.7	1.44, br s	18.7	1.43, d (6.8)	18.2	1.03, d (7.0)	18.5	1.09, d (7.0)	18.5	1.04, d (7.0)
11-OH		6.82, s		5.58, s		3.39, d (3.0)		3.37, d (2.9)		3.20, d (3.2)
3-SMe					13.8	2.11, s	13.8	2.11, s	13.9	2.11, s
6-NMe									33.1	2.53, s
12-SMe					16.5	1.96, s	16.4	1.96, s	16.5	1.95, s
1′	165.5		170.3		165.8		165.9		165.9	
3′	75.4		78.5		71.0		71.6		71.0	
4′	163.1		167.8		163.8		163.4		163.8	
5a′	77.0	5.67, s	79.1	6.56, d (2.0)	78.1	6.03, d (2.3)	83.9	6.10, s	78.0	6.00, d (2.6)
6′		4.48, s		4.84, s		4.83, d (2.3)				
6a′	151.0		149.8		150.1		152.2		150.0	
7′	110.2	6.52, d (7.3)	107.9	6.41, d (7.8)	108.8	6.56, d (7.8)	105.7	6.37, d (7.5)	108.7	6.59, d (7.8)
8′	130.2	7.26, t (7.3)	129.7	6.98, t (7.6)	129.6	7.07, td (7.7, 1.8)	129.8	7.10, td (7.5, 1.8)	129.7	7.03, td (7.7, 1.2)
9′	119.6	6.98, t (7.6)	118.1	6.28, t (7.4)	118.2	6.35, t (7.7)	118.4	6.27, td (7.5, 1.0)	118.1	6.34, td (7.6, 1.0)
10′	128.1	7.70, d (7.0)	128.9	5.85, d (7.6)	128.4	5.78, d (8.0)	128.1	5.70, dd (7.6, 1.0)	128.5	5.70, d (7.6)
10a′	124.0		122.8		123.0		123.3		123.0	
10b′	64.4		60.0		61.0		60.0		61.1	
11′	75.8	5.72, s	79.9	5.63, d (3.4)	79.6	5.41, d (11.4)	80.0	5.33, d (10.2)	79.6	5.38, d (11.4)
12′	77.4		78.5		73.7		73.6		73.7	
13′	27.5	3.15, s	28.7	3.11, s	28.7	3.15, s	28.7	3.15, s	28.7	3.14, s
14′a	60.7	4.23, dd (7.9, 10.2)	62.9	4.04, d (12.4)	64.2	3.89, d (12.1)	64.1	3.87, d (12.0)	64.3	3.89, d (12.0)
14′b		4.36, dd (4.3, 10.2)		4.38, d (12.4)		4.34, d (12.1)		4.35, d (12.0)		4.34, d (12.0)
11′-OH		5.14, s		3.59, d (3.5)		3.15, d (11.4)		3.09, d (10.2)		3.12, d (11.5)
14′-OH		3.45, dd (4.3, 7.9)				5.03, s		5.01, d (1.2)		
3′-SMe					14.0	2.25, s	14.0	2.25, s	14.0	2.25, s
6′-NMe							32.1	3.05, s		
12′-SMe					16.1	1.98, s	16.1	1.99, s	16.0	1.98, s

[a]Recorded in $CDCl_3$ at 25 °C.

dx.doi.org/10.1021/np5002253 | J. Nat. Prod. 2014, 77, 1459−1466

Table 2. Inhibition of *in Vitro* Cancer Cell Lines by Preussiadin A (1)[a]

cell line	GI_{50} (nM)[b]	TGI (nM)[c]	LC_{50} (nM)[d]	cell line	GI_{50} (nM)[b]	TGI (nM)[c]	LC_{50} (nM)[d]
Leukemia				Melanoma			
CCRF-CEM	9.3	38.0	>50 000	M14	13.5	53.7	182.0
HL-60 (TB)	26.3	195.0	>50 000	MDA-MB-435	10.7	28.8	120.2
K-562	14.8	114.8	>50 000	SK-MEL-2	9.8	20.4	43.7
MOLT-4	13.2	67.6	>50 000	SK-MEL-28	12.6	38.0	134.9
RPMI-8226	12.3	34.7	>50 000	SL-MEL-5	14.8	57.5	151.4
SR	11.2	31.6	>50 000	UACC-257	8.7	19.5	43.7
Non-Small Cell Line Cancer				UACC-62	18.2	72.4	295.1
A549/ATCC	26.3	93.3	263.0	Ovarian Cancer			
EKVX	28.2	257.0	2041.7	IGROV1	24.5	100.0	338.8
HOP-62	11.7	30.9	109.6	OVCAR-3	10.7	26.3	85.1
HOP-92	11.0	28.8	112.2	OVCAR-4	5.9	12.9	27.5
NCI-H226	10.0	24.0	72.4	OVCAR-5	52.5	138.0	363.1
NCI-H23	16.2	56.2	234.4	OVCAR-8	9.5	19.1	38.0
NCI-H322M	20.0	102.3	489.8	NCI/ADR-RES	33.9	120.2	354.8
NCI-H460	20.9	75.9	245.5	SK-OV-3	11.5	33.9	190.5
NCI-H522	8.5	17.8	38.0	Renal Cancer			
Colon Cancer				786-0	11.7	26.3	70.8
COLO 205	14.8	49.0	154.9	A498	9.8	28.2	104.7
HCC-2998	53.7	114.8	245.5	ACHN	15.5	60.3	234.4
HCT-116	12.3	51.3	162.2	CAKI-1	8.7	22.4	85.1
HCT-15	17.0	89.1	478.6	RXF 393	7.8	14.8	28.2
HT29	5.6	13.5	32.4	SN12C	22.9	524.8	1778.3
KM12	19.5	87.1	295.1	TK-10	11.7	24.5	57.5
SW-620	8.3	31.6	128.8	UO-31	9.8	26.3	100.0
CNS Cancer				Prostate Cancer			
SF-268	22.4	107.2	416.9	PC-3	15.5	60.3	208.9
SF-295	57.5	154.9	416.9	DU-145	14.8	53.7	199.5
SF-539	15.1	58.9	199.5	Breast Cancer			
SNB-19	112.2	512.9	1659.6	MCF7	10.0	55.0	166.0
SNB-75	13.5	50.1	158.5	MDA-MB-231/ATCC	18.6	70.8	323.6
U251	17.8	61.7	177.8	HS 578T	26.3	446.7	NT[e]
Melanoma				BT-549	14.8	66.1	208.9
LOX IMVI	8.3	21.4	46.8	T-47D	9.1	26.3	102.3
MALME-3M	7.8	18.6	45.7				

[a]Data obtained from the NCI-60 cell line panel. [b]GI_{50} is the molar concentration causing 50% growth inhibition of tumor cells. [c]TGI is the molar concentration giving total growth inhibition. [d]LC_{50} is the molar concentration leading to 50% net cell death. [e]Not tested.

no cytotoxic effects against the MIA PaCa-2 cells at concentrations of up to 30 μM. These results further support the importance of the polythioether bridge for triggering mammalian cell toxicity.

To further elaborate the scope of activity for compound **1**, it was evaluated in the NCI-60 *in vitro* drug screening program. Compound **1** exhibited potent antiproliferative activity against each of the 60 cell lines with an average GI_{50} value of 14.8 nM (Table 2). Compound **1** also exhibited cytotoxic effects against all of the solid tumor cell lines with an average LC_{50} of 251 nM; however, it was not cytotoxic against the six leukemia cell lines, indicating that **1** exhibited some degree of selectivity.

A common mechanism of multidrug resistance is the expression of the P-glycoprotein (Pgp) transporter, the product of the *MDR1* gene. Efflux of drug molecules through this transporter contributes to development of innate and acquired drug resistance, including resistance to many structurally complex natural products.[22] The ability of **1** to circumvent Pgp-mediated drug resistance was studied using an isogenic cell line pair, the parental SK-OV-3 line and the Pgp-expressing clone SK-OV-3/MDR-1-M6/6 (M6/6).[23] The dose–response curves for **1** and paclitaxel, a known Pgp substrate, are shown in Figure 5A. The relative resistance values, indicating the effects of Pgp expression, were calculated by dividing the GI_{50} of **1** in the Pgp-expressing M6/6 line by the GI_{50} obtained in the parental SK-OV-3 line.[24] As expected, paclitaxel was significantly less potent against the Pgp-expressing cell line and had a relative resistance value of 127 (Figure 5). In contrast, **1** had a relative resistance of 1.7, indicating that it was a poor Pgp substrate (Figure 5).[25] These results are consistent with the NCI-60 data, where **1** was effective against the Pgp-expressing NCI/ADR-RES cell line.[26−28] These results indicate that **1** overcomes Pgp-mediated drug resistance.

Cellular persistence evaluates the long-term effects of a short exposure of cells to a drug. Although it is unclear whether high cellular persistence is a desired property of anticancer agents, recent studies have demonstrated that it can be a predictor of high *in vivo* efficacy.[29,30] The cellular persistence of **1** was evaluated in a clonogenic assay using UACC-62 melanoma cells, which was one of the most sensitive cell lines evaluated in the NCI-60 panel, as well as HeLa cells. The cells were exposed to different concentrations of **1** for 4 h, washed to remove residual compound, and allowed to form colonies for 14 days. A 4 h exposure of cells to **1** caused a dose-dependent inhibition of colony formation, with 5 nM **1** reducing colony formation by 38% as compared to vehicle-treated cells (p = 0.0286) (Figure 6).

dx.doi.org/10.1021/np5002253 | J. Nat. Prod. 2014, 77, 1459−1466

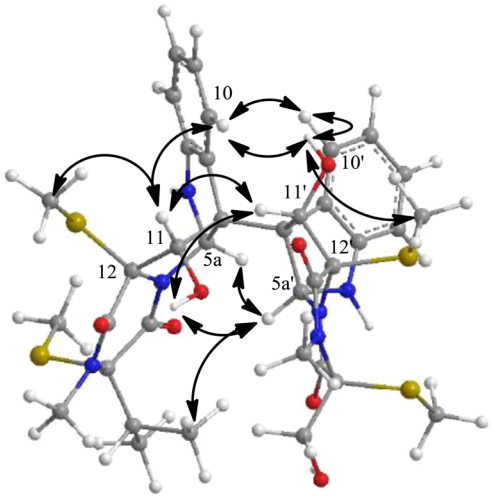

Figure 1. Key ROESY correlations for **3**.

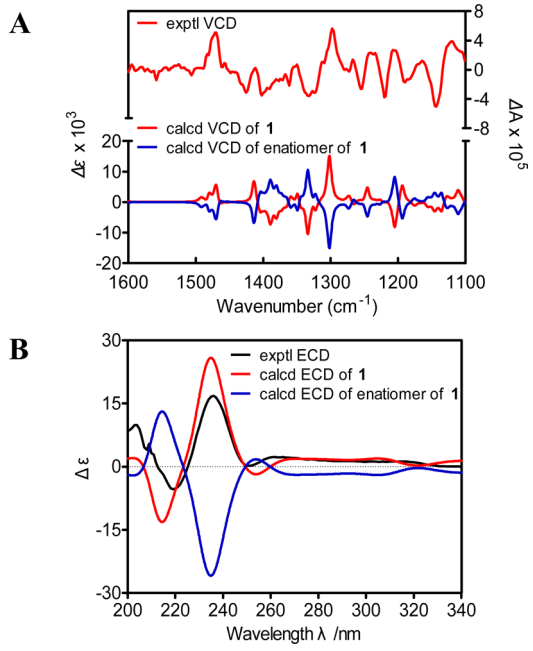

Figure 2. Comparison of experimental and calculated VCD (A) and ECD (B) spectra of **1**.

Similar results were also obtained in experiments using HeLa cells (data not shown). A previous study by our group using a similar experimental design demonstrated that cellular persistence of a compound after 4 h of treatment can vary dramatically for different cytotoxic agents, indicating that this effect is specific to **1** and not a general effect of all cytotoxins.[31] These results suggest that the cellular effects of **1** are highly persistent and that short exposure times are sufficient to induce cytotoxicity.

The COMPARE algorithm[32] was used to evaluate the potential mechanism of action of **1**. The results indicated that **1** might share a mechanism of action with the mTORC1 inhibitor rapamycin and other mTORC inhibitors. To determine whether **1** is capable of inhibiting cellular mTORC1 signaling, whole-cell lysates of vehicle and **1**-treated HeLa cells (HeLa GI_{50} = 20 nM) were analyzed by Western blotting to determine the relative levels of phosphorylation of S6 kinase (S6K), a major downstream effector of mTORC1. While the known mTORC1 inhibitor rapamycin (100 nM) completely inhibited phosphorylation of the T389 residue of S6K, **1** had no effect on this phosphorylation at concentrations up to 100 nM (Figure S22). This finding indicates that **1** does not inhibit signaling through the mTORC1 pathway at cytotoxic concentrations to HeLa and other cancer cell lines. This suggests that mTORC1 inhibition is not involved in the mechanism of action of **1**.

It has previously been reported that chaetocin, a compound with structural similarity to **1**, inhibits the di- and trimethylation of histone H3 lysine 9 (H3K9) by targeting the lysine methyltransferase SU(VAR)3-9.[33] Another recent report suggested that chaetocin may nonspecifically inhibit lysine methyltransferases.[34] The effects of **1** on H3K9 methylation were studied in HeLa cells treated with vehicle or 200 nM **1** for 1−24 h. The relative levels of trimethylated H3K9 (H3K9me3) were evaluated by immunoblotting. The results indicated that **1** did not cause a decrease of H3K9me3 levels, but actually caused higher expression of H3K9me3 (Figure S23). This increase is likely an indirect result of suppression of transcription as cells begin to die.

The antitumor effects of **1** were evaluated in a UACC-62 xenograft mouse model. On the basis of the high level of cellular persistence of **1**, it was expected that this compound could be administered infrequently while retaining efficacy. Initial dose−tolerance testing was conducted with 10 mg/kg of **1**, but this dose caused rapid and persistent weight loss of 5−10%. Further studies showed that two or more doses of **1** at 2 mg/kg also caused rapid and persistent weight loss. A dose of 1.5 mg/kg every 4 days was determined to be the maximum tolerated dose and was used for antitumor efficacy studies. With this dosing schedule, **1** slightly inhibited tumor growth (T/C% = 67%) and reduced final tumor volume relative to untreated control mice, but this effect was not statistically significant (p = 0.2896; Figure S24). The results of this study indicate that **1** may have antitumor efficacy *in vivo*, but it has a very narrow therapeutic window.

EXPERIMENTAL SECTION

General Experimental Procedures. Optical rotations were measured on a Rudolph Research Autopol III automatic polarimeter. UV data were measured with a Hewlett-Packard 8452A diode array spectrophotometer. ECD spectra were recorded on a model 202-01 AVIV circular dichroism spectrometer. IR spectra were measured on a Bruker Vector 22 FT-IR spectrometer. NMR data were obtained on a Varian VNMR spectrometer (400 MHz for ^{1}H and 2D NMR, 100 MHz for ^{13}C NMR) with a broad band resonance probe. Electrospray-ionization mass spectrometry data were collected on an Agilent 6538 high-mass-resolution QTOF mass spectrometer. HPLC separations were performed on a Shimadzu system using an SCL-10A VP system controller and a Gemini 5 μm C_{18} column (110 Å, 250 × 21.2 mm and 250 × 10.0 mm) with flow rates of 10 or 4 mL/min. All solvents were of ACS grade or better.

Fermentation, Extraction, and Isolation. The identification of *P. typharum* (Sacc.) Cain (GenBank accession JX143871), its fermentation on Cheerios breakfast cereal, and extraction procedures were described previously.[16] The crude extract (100 g) was separated into nine fractions by silica column chromatography (eluted with a gradient of hexanes−dichloromethane and dichloromethane−MeOH). Fraction 7 was further separated into three subfractions by C_{18} vacuum column chromatography. Fraction 7-2 was subjected to repeated Sephadex LH20 column chromatography (eluted with dichloromethane−MeOH, 1:1) and silica preparative TLC (hexanes−EtOAc) to yield compounds **6** (66 mg, 0.066% yield) and **7** (10 mg, 0.010%

dx.doi.org/10.1021/np5002253 | J. Nat. Prod. 2014, 77, 1459−1466

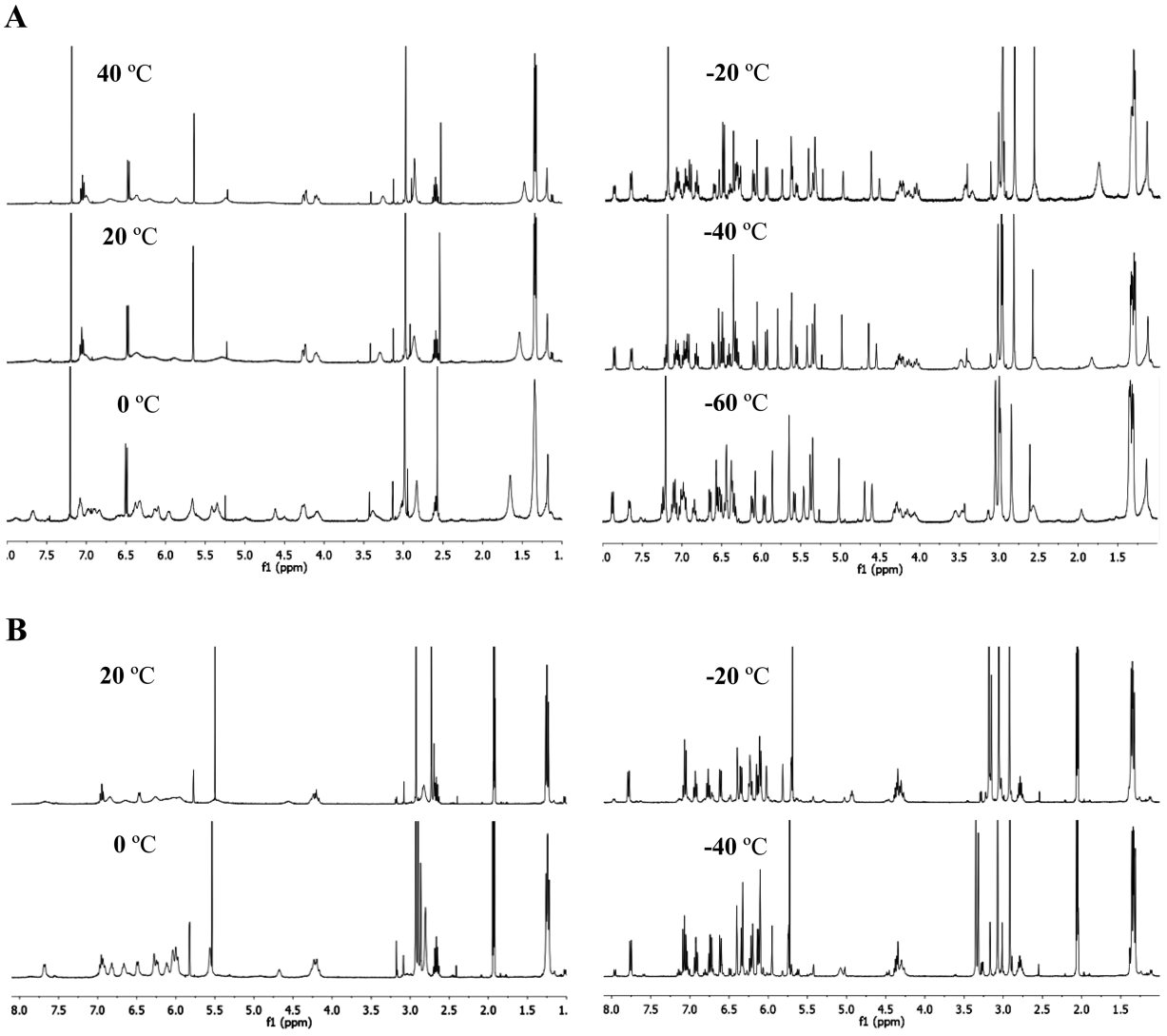

Figure 3. Variable-temperature ^{1}H NMR experiments of **6** in $CDCl_3$ (A) and acetone-d_6 (B).

A

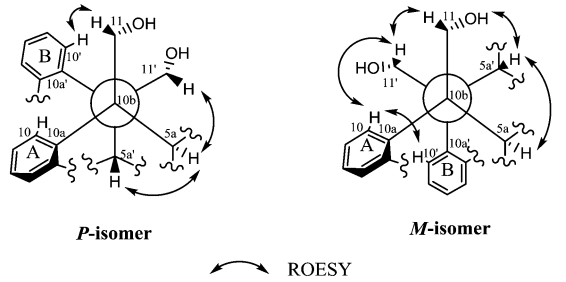

B

No.	1[a]	2[a]	3[a]	4[a]	5[a]	6[b]	7[a]
10	5.71	7.55	7.72	7.67	7.65	7.79	5.59
10'	7.70	5.85	5.78	5.70	5.70	6.14	7.85

[a]Recorded in $CDCl_3$ at 25 °C. [b]Recorded in acetone-d_6 at -20 °C.

Figure 4. Key ROESY correlations for **1** (*P*-isomer), **2**, and **3** (*M*-isomer) (A) and selected ^{1}H NMR data for **1**−**7** (B).

yield). Subfraction 7-2-3-4 was further subjected to semipreparative HPLC (Luna 5 μm, C_8, 110 Å, 250 × 10.00 mm, MeCN−H_2O, 55:45, 4.0 mL/min) to yield **1** (10 mg, 0.010% yield) and **2** (3.6 mg, 0.0036% yield).

*Preussiadin A (**1**):* white powder; $[\alpha]^{24}_D$ 66 (*c* 0.1, $CHCl_3$); UV (EtOH) λ_{max} (log ε) 208 (4.55), 300 (3.59); IR (film) ν_{max} 3399, 2966, 2935, 1673, 1482, 1463, 1351, 1315, 1248, 1217, 1140, 1061 cm^{-1}; CD (EtOH) λ_{max} ($\Delta\varepsilon$) 219 (−5.3), 236 (16.8), 262 (2.3), 313 (1.2); ^{1}H and ^{13}C NMR data in Tables 1 and 2, respectively; HRESIMS *m*/*z* 763.1102, $[M + Na]^+$ (calcd for $C_{32}H_{32}N_6O_7S_4Na$, 763.1108).

*Preussiadin B (**2**):* white powder; $[\alpha]^{24}_D$ 34 (*c* 0.1, $CHCl_3$); UV (EtOH) λ_{max} (log ε) 210 (4.79), 300 (3.69); IR (film) ν_{max} 3399, 2962, 2928, 1664, 1474, 1455, 1418, 1373, 1313, 1261, 1216, 1096, 1066 cm^{-1}; CD (EtOH) λ_{max} ($\Delta\varepsilon$) 212 (20.6), 234 (18.2), 268 (−8.5), 335 (1.2); ^{1}H and ^{13}C NMR data in Tables 1 and 2, respectively; HRESIMS *m*/*z* 827.0556, $[M + Na]^+$ (calcd for $C_{32}H_{32}N_6O_7S_6Na$, 827.0549).

Computational Details. The conformational analysis was carried out using Spartan'10. Geometry, frequency, IR and VCD intensity, UV and ECD spectra, and specific rotation calculations were applied at the DFT level with Gaussian 09. ComputeVOA v0.1 was used to sum IR or VCD spectra after a Boltzmann statistical weighting. UV and ECD spectra were added based on Boltzmann distribution using SpecDis 1.60. The assignment based on VCD comparison was evaluated using the CompareVOA program.[35] The confidence level of the assignment for the proposed absolute configuration of **1** is 95% based on its current database, which includes 105 previous correct assignments for different chiral structures.

Formation of the Tetrakis(methylsulfanyl) Derivatives 3−5. Preussiadin A (**1**) (13 mg) was dissolved in 0.26 mL of pyridine−MeOH (5:8). MeI (1 mL) and $NaBH_4$ (5 mg) were added, and the mixture was stirred for 20 min at room temperature. The reaction mixture was then diluted with water and extracted with EtOAc. The

dx.doi.org/10.1021/np5002253 | J. Nat. Prod. 2014, 77, 1459−1466

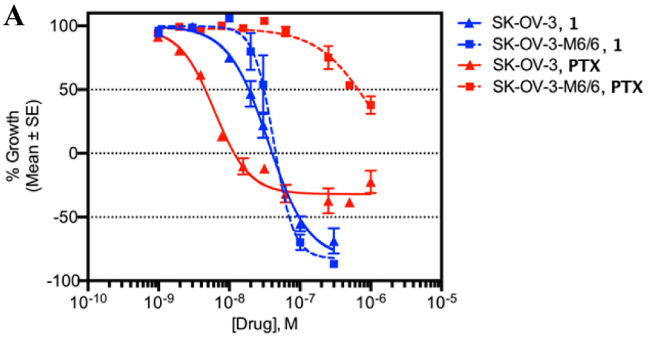

B

Cell line	GI_{50}, nM (Mean ± SE)	
	Compound 1	Paclitaxel
SK-OV-3	19 ± 3	4.7 ± 0.3
SK-OV-3-M6/6	33 ± 7	600 ± 200
Rr	1.7	127

Figure 5. (A) Dose–response curves for growth inhibition of SK-OV-3 and SK-OV-3-M6/6 cells following treatment with **1** or paclitaxel (PTX). Data represent mean ± SE for n = 1–4 independent experiments. When not visible, error bars are contained within the boundaries of the data points, except for PTX treatment at 30 and 250 nM (n = 1). (B) GI_{50} values for **1** and PTX in SK-OV-3 and SK-OV-3-M6/6 cells and their respective relative resistance (Rr) values. Results represent n = 3 or 4 independent experiments.

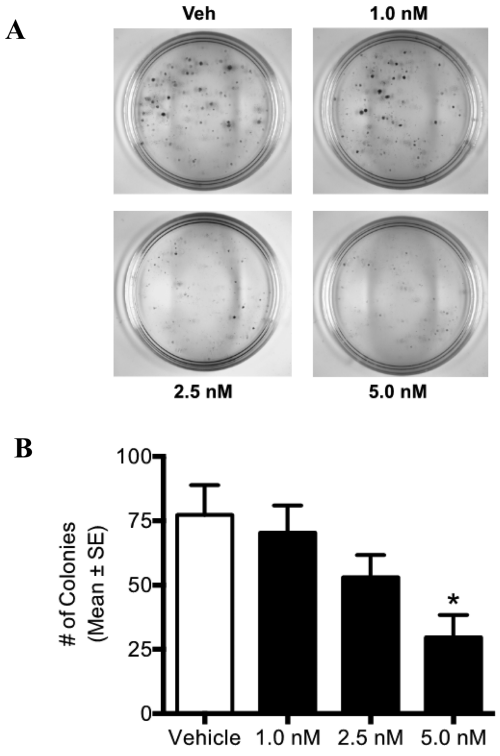

Figure 6. (A) Representative images of crystal violet-stained UACC-62 colonies 14 days after 4 h of treatment with vehicle or various concentrations of **1**. (B) Quantification of UACC-62 colony number. Results represent n = 2–4 independent experiments, with each concentration tested in duplicate or triplicate. *p < 0.05 compared to vehicle determined by one-way ANOVA and Dunnett's *post hoc* test.

solvent was evaporated under reduced pressure, and the residue was separated on a preparative silica TLC plate with hexanes–EtOAc (7:4) as an eluent. The products were further purified by semipreparative HPLC using MeOH–H_2O (4:1) to afford **3** (2.6 mg), **4** (2.1 mg), and **5** (0.5 mg). The same reaction with **2** (2.0 mg) gave **3** (0.7 mg), as well as **4** and **5** in trace amounts.

*Preussiadin A_1 (**3**):* white powder; $[\alpha]^{24}_D$ −14.2 (c 0.14, $CHCl_3$); UV (EtOH) λ_{max} (log ε) 208 (4.55), 244 (sh, 3.98), 306 (3.56); IR (film) ν_{max} 3378, 2966, 2935, 1655, 1484, 1457, 1420, 1383, 1317, 1259, 1205, 1088 cm^{-1}; CD (EtOH) λ_{max} ($\Delta\varepsilon$) 212 (16.0), 237 (sh, 1.3), 254 (−10.5), 305 (−0.3), 324 (−0.8); ^1H and ^{13}C NMR data in Tables 1 and 2, respectively; HRESIMS m/z 823.2053, $[M + Na]^+$ (calcd for $C_{36}H_{44}N_6O_7S_4Na$, 823.2047).

*Preussiadin A_2 (**4**):* white powder; $[\alpha]^{24}_D$ −30 (c 0.12, $CHCl_3$); UV (EtOH) λ_{max} (log ε) 210 (4.60), 248 (sh, 4.03), 308 (3.58); IR (film) ν_{max} 3396, 2967, 2924, 1654, 1488, 1419, 1382, 1308, 1254, 1196, 1123, 1096, 1047 cm^{-1}; CD (EtOH) λ_{max} ($\Delta\varepsilon$) 212 (28.0), 239 (sh, 3.0), 258 (−10.0), 301 (2.5), 326 (−2.3); ^1H and ^{13}C NMR data in Tables 1 and 2, respectively; HRESIMS m/z 837.2213, $[M + Na]^+$ (calcd for $C_{37}H_{46}N_6O_7S_4Na$, 837.2203).

*Preussiadin A_3 (**5**):* white powder; $[\alpha]^{24}_D$ −32 (c 0.03, $CHCl_3$); UV (EtOH) λ_{max} (log ε) 210 (4.65), 248 (sh, 4.10), 308 (3.65); IR (film) ν_{max} 3408, 2966, 2927, 1655, 1464, 1422, 1382, 1306, 1260, 1199, 1133, 1083, 1045 cm^{-1}; CD (EtOH) λ_{max} ($\Delta\varepsilon$) 208 (6.6), 219 (−2.3), 227 (2.2), 235 (−1.0), 243 (1.9), 257 (−11.8), 292 (−2.9), 326 (2.4); ^1H and ^{13}C NMR data in Tables 1 and 2, respectively; HRESIMS m/z 837.2212, $[M + Na]^+$ (calcd for $C_{37}H_{46}N_6O_7S_4Na$, 837.2203).

Cell Culture. MIA PaCa-2, SK-OV-3, and HeLa cell lines were obtained from ATCC and cultured as previously described.[24,36] UACC-62 cells were obtained from AddexBio and cultured in RPMI-1640 media (Sigma-Aldrich) supplemented with 10% fetal bovine serum and 50 μg/mL gentamicin reagent (Gibco). The SK-OV-3/MDR-1-6/6 cell line is derived from a single cell clone from the SK-OV-3/MDR1 cell line obtained from S. Kane (Division of Molecular Medicine, Beckman Research Institute of the City of Hope, Duarte, CA, USA) and cultured as previously described.[23]

***In Vitro* Antiproliferative/Cytotoxicity Assays.** The MTT assay with MIA PaCa-2 cells and the calculation of IC_{50} values were performed as previously described.[36] The *in vitro* antiproliferative and cytotoxic effects in SK-OV-3 and SK-OV-3/MDR-1-6/6 cells were tested using the sulforhodamine B (SRB) assay.[37] The GI_{50}, TGI, and LC_{50} values reported were calculated from the dose–response curves for percent cell growth using GraphPad Prism 6. Percent cell growth was calculated as previously described by Boyd et al.[37] Results represent the mean ± standard error.

***In Vitro* Clonogenic Assays.** UACC-62 cells (600) or HeLa cells (300) were allowed to adhere in 60 mm^3 tissue culture dishes and subsequently treated with vehicle (DMSO) or **1**. After 4 h of treatment, cells were washed with Dulbecco's phosphate-buffered saline (DPBS) and fresh growth medium was added. After 14 days, cells were fixed and stained with 0.5% crystal violet in 10% methanol. Colonies were counted using GeneSnap software (PerkinElmer). Data were analyzed by one-way ANOVA with Dunnett's *post hoc* test using GraphPad Prism 6.

Immunoblotting/Cell Lysates. HeLa cells in log-phase growth were harvested and lysed with cell extraction buffer (Invitrogen) containing protease inhibitors. Total protein concentrations were measured, and equal amounts of protein were separated by SDS-PAGE and transferred to a PVDF membrane. Membranes were probed for actin (Sigma-Aldrich), S6 kinase (Cell Signaling), P-T389-S6 kinase (Cell Signaling), or H3K9me3 (Abcam). Signals were visualized with Amersham ECL Plus (GE Health Care) in a Geliance (PerkinElmer) imaging system.

Xenograft Studies. Female athymic nude mice were obtained from Jackson Laboratories and housed in an AAALAC approved facility at the University of Texas Health Science Center at San Antonio. Mice were transplanted bilaterally with 2 × 10^6 UACC-62 cells injected sc into each flank. They were randomized (n = 5 mice/group) after tumors reached a median volume of 150 mm^3. Compound **1** was dissolved in DMSO–Cremophor (1:1) and administered *ip* after diluting in 200 μL of DPBS (maximum final concentration of DMSO and Cremophor was 2.5%). Mice were weighed and examined daily for tumor growth. Tumors were measured twice weekly using calipers, and tumor volume was calculated using the following formula: volume

dx.doi.org/10.1021/np5002253 | J. Nat. Prod. 2014, 77, 1459–1466

(mm^3) = length (mm) × width (mm) × height (mm). Data for final tumor volume after 14 days postimplantation were analyzed by a two-tailed *t*-test using GraphPad Prism 6. T/C% was calculated using the formula [mean final tumor volume (treated) − mean initial tumor volume (treated)] ÷ [mean final tumor volume (untreated) − mean initial tumor volume (untreated)] × 100.

■ ASSOCIATED CONTENT

Supporting Information

NMR data tables for **1**−**3** (^{1}H and ^{13}C NMR, HMBC, and ROESY), NMR spectra of **1**−**3** (^{1}H and ^{13}C NMR, HSQC, HMBC, and ROESY) and **4** and **5** (^{1}H and ^{13}C NMR), computational conformation analysis and DFT-calculated spectral data (VCD and specific rotations) of **1** are available. This material is available free of charge via the Internet at http://pubs.acs.org.

■ AUTHOR INFORMATION

Corresponding Authors

*E-mail: mooberry@uthscsa.edu.

*E-mail: rhcichewicz@ou.edu.

Author Contributions

⊥L. Du and A. J. Robles contributed equally.

Notes

The authors declare no competing financial interest.

■ ACKNOWLEDGMENTS

Research reported in this publication was supported by the National Institute of General Medical Sciences of the National Institutes of Health, RO1GM092219 (R.H.C.), the President's Council Excellence Award (S.L.M.), and the Greehey President's Endowment (S.L.M.). The X-ray diffractometer was purchased through a grant from the NSF (CHE-0130835). The LC-MS instrument used for this project was provided in part by a Challenge Grant from the Office of the Vice President for Research, University of Oklahoma, Norman Campus, and an award through the Shimadzu Equipment Grant Program (R.H.C.).

■ REFERENCES

(1) Iwasa, E.; Hamashima, Y.; Sodeoka, M. *Isr. J. Chem.* **2011**, *51*, 420−433.

(2) Boyer, N.; Morrison, K. C.; Kim, J.; Hergenrother, P. J.; Movassaghi, M. *Chem. Sci.* **2013**, *4*, 1646−1657.

(3) Rether, J.; Serwe, A.; Anke, T.; Erkel, G. *Biol. Chem.* **2007**, *388*, 627−637.

(4) Isham, C. R.; Tibodeau, J. D.; Bossou, A. R.; Merchan, J. R.; Bible, K. C. *Br. J. Cancer* **2012**, *106*, 314−323.

(5) Chaib, H.; Nebbioso, A.; Prebet, T.; Castellano, R.; Garbit, S.; Restouin, A.; Vey, N.; Altucci, L.; Collette, Y. *Leukemia* **2012**, *26*, 662−674.

(6) Isham, C. R.; Tibodeau, J. D.; Jin, W.; Xu, R. F.; Timm, M. M.; Bible, K. C. *Blood* **2007**, *109*, 2579−2588.

(7) Liu, F. Y.; Liu, Q. Q.; Yang, D. F.; Bollag, W. B.; Robertson, K.; Wu, P.; Liu, K. B. *Cancer Res.* **2011**, *71*, 6807−6816.

(8) Cook, K. M.; Hilton, S. T.; Mecinovic, J.; Motherwell, W. B.; Figg, W. D.; Schofield, C. J. *J. Biol. Chem.* **2009**, *284*, 26831−26838.

(9) Yanagihara, M.; Sasaki-Takahashi, N.; Sugahara, T.; Yamamoto, S.; Shinomi, M.; Yamashita, L.; Hayashida, M.; Yamanoha, B.; Numata, A.; Yamori, T.; Andoh, T. *Cancer Sci.* **2005**, *96*, 816−824.

(10) Lee, Y. M.; Lim, J. H.; Yoon, H.; Chun, Y. S.; Park, J. W. *Hepatology* **2011**, *53*, 171−180.

(11) Iwasa, E.; Hamashima, Y.; Fujishiro, S.; Higuchi, E.; Ito, A.; Yoshida, M.; Sodeoka, M. *J. Am. Chem. Soc.* **2010**, *132*, 4078−4079.

(12) Dubey, R.; Levin, M. D.; Szabo, L. Z.; Laszlo, C. F.; Kushal, S.; Singh, J. B.; Oh, P.; Schnitzer, J. E.; Olenyuk, B. Z. *J. Am. Chem. Soc.* **2013**, *135*, 4537−4549.

(13) Block, K. M.; Wang, H.; Szabo, L. Z.; Polaske, N. W.; Henchey, L. K.; Dubey, R.; Kushal, S.; Laszlo, C. F.; Makhoul, J.; Song, Z. H.; Meuillet, E. J.; Olenyuk, B. Z. *J. Am. Chem. Soc.* **2009**, *131*, 18078−18088.

(14) Greiner, D.; Bonaldi, T.; Eskeland, R.; Roemer, E.; Imhof, A. *Nat. Chem. Biol.* **2005**, *1*, 143−145.

(15) Figueroa, M.; Graf, T. N.; Ayers, S.; Adcock, A. F.; Kroll, D. J.; Yang, J.; Swanson, S. M.; Munoz-Acuna, U.; Carcache de Blanco, E. J.; Agrawal, R.; Wani, M. C.; Darveaux, B. A.; Pearce, C. J.; Oberlies, N. H. *J. Antibiot.* **2012**, *65*, 559−564.

(16) Du, L.; King, J. B.; Morrow, B. H.; Shen, J. K.; Miller, A. N.; Cichewicz, R. H. *J. Nat. Prod.* **2012**, *75*, 1819−1823.

(17) Takahashi, C.; Numata, A.; Ito, Y.; Matsumura, E.; Araki, H.; Iwaki, H.; Kushida, K. *J. Chem. Soc., Perkin Trans. 1* **1994**, 1859−1864.

(18) Shao, Y.; Molnar, L. F.; Jung, Y.; Kussmann, J.; Ochsenfeld, C.; Brown, S. T.; Gilbert, A. T. B.; Slipchenko, L. V.; Levchenko, S. V.; O'Neill, D. P.; DiStasio, R. A.; Lochan, R. C.; Wang, T.; Beran, G. J. O.; Besley, N. A.; Herbert, J. M.; Lin, C. Y.; Van Voorhis, T.; Chien, S. H.; Sodt, A.; Steele, R. P.; Rassolov, V. A.; Maslen, P. E.; Korambath, P. P.; Adamson, R. D.; Austin, B.; Baker, J.; Byrd, E. F. C.; Dachsel, H.; Doerksen, R. J.; Dreuw, A.; Dunietz, B. D.; Dutoi, A. D.; Furlani, T. R.; Gwaltney, S. R.; Heyden, A.; Hirata, S.; Hsu, C. P.; Kedziora, G.; Khalliulin, R. Z.; Klunzinger, P.; Lee, A. M.; Lee, M. S.; Liang, W.; Lotan, I.; Nair, N.; Peters, B.; Proynov, E. I.; Pieniazek, P. A.; Rhee, Y. M.; Ritchie, J.; Rosta, E.; Sherrill, C. D.; Simmonett, A. C.; Subotnik, J. E.; Woodcock, H. L.; Zhang, W.; Bell, A. T.; Chakraborty, A. K.; Chipman, D. M.; Keil, F. J.; Warshel, A.; Hehre, W. J.; Schaefer, H. F.; Kong, J.; Krylov, A. I.; Gill, P. M. W.; Head-Gordon, M. *Phys. Chem. Chem. Phys.* **2006**, *8*, 3172−3191.

(19) Biddanda, B. A.; Cotner, J. B. *Ecosystems* **2002**, *5*, 431−445.

(20) Bruhn, T.; Schaumloffel, A.; Hemberger, Y.; Bringmann, G. *Chirality* **2013**, *25*, 243−249.

(21) Saito, T.; Suzuki, Y.; Koyama, K.; Natori, S.; Iitaka, Y.; Kinoshita, T. *Chem. Pharm. Bull.* **1988**, *36*, 1942−1956.

(22) Borst, P.; Elferink, R. O. *Annu. Rev. Biochem.* **2002**, *71*, 537−592.

(23) Sadava, D.; Coleman, A.; Kane, S. E. *J. Liposome Res.* **2002**, *12*, 301−309.

(24) Risinger, A. L.; Jackson, E. M.; Polin, L. A.; Helms, G. L.; LeBoeuf, D. A.; Joe, P. A.; Hopper-Borge, E.; Luduena, R. F.; Kruh, G. D.; Mooberry, S. L. *Cancer Res.* **2008**, *68*, 8881−8888.

(25) Ruiz Gomez, M. J.; Gil, L.; Souviron, A.; Martinez Morillo, M. *J. Physiol. Biochem.* **2000**, *56*, 33−38.

(26) Ke, W.; Yu, P.; Wang, J.; Wang, R.; Guo, C.; Zhou, L.; Li, C.; Li, K. *Med. Oncol.* **2011**, *28* (Suppl1), S135−S141.

(27) Liscovitch, M.; Ravid, D. *Cancer Lett.* **2007**, *245*, 350−352.

(28) Vickers, P. J.; Dickson, R. B.; Shoemaker, R.; Cowan, K. H. *Mol. Endocrinol.* **1988**, *2*, 886−892.

(29) Risinger, A. L.; Li, J.; Bennett, M. J.; Rohena, C. C.; Peng, J.; Schriemer, D. C.; Mooberry, S. L. *Cancer Res.* **2013**, *73*, 6780−6792.

(30) Towle, M. J.; Salvato, K. A.; Wels, B. F.; Aalfs, K. K.; Zheng, W.; Seletsky, B. M.; Zhu, X.; Lewis, B. M.; Kishi, Y.; Yu, M. J.; Littlefield, B. A. *Cancer Res.* **2011**, *71*, 496−505.

(31) Risinger, A. L.; Mooberry, S. L. *Cell Cycle* **2011**, *10*, 2162−2171.

(32) Gharehbaghi, K.; Sreenath, A.; Hao, Z.; Paull, K. D.; Szekeres, T.; Cooney, D. A.; Krohn, K.; Jayaram, H. N. *Biochem. Pharmacol.* **1994**, *48*, 1413−1419.

(33) Greiner, D.; Bonaldi, T.; Eskeland, R.; Roemer, E.; Imhof, A. *Nat. Chem. Biol.* **2005**, *1*, 143−145.

(34) Cherblanc, F. L.; Chapman, K. L.; Brown, R.; Fuchter, M. J. *Nat. Chem. Biol.* **2013**, *9*, 136−137.

(35) Debie, E.; De Gussem, E.; Dukor, R. K.; Herrebout, W.; Nafie, L. A.; Butinck, P. *ChemPhysChem* **2011**, *12*, 1542−1549.

(36) Wang, X. R.; You, J. L.; King, J. B.; Powell, D. R.; Cichewicz, R. H. *J. Nat. Prod.* **2012**, *75*, 707−715.

(37) Boyd, M. R.; Paull, K. D.; Rubinstein, L. R. In *Cytotoxic Anticancer Drugs: Models and Concepts for Drug Discovery and Development*; Valeriote, F. A.; Corbett, T.; Baker, L., Ed.; Kluwer Academic Publishers: Amsterdam, 1992; pp 11−34.